Supplementary Material for "Uncalibrated Photometric Stereo by Stepwise Optimization Using Principal Components of Isotropic BRDFs"

Keisuke Midorikawa Toshihiko Yamasaki Kiyoharu Aizawa
The University of Tokyo, Japan
{k.midor, yamasaki, aizawa}@hal.t.u-tokyo.ac.jp

1. Rotation/Flip Disambiguation by Enforcing Integrability

As mentioned in the end of Sec. 3.1, the result of minimizing Eq. (4) has the rotation/flip ambiguity. This is because isotropic BRDFs depend only on the relative directions among surface normals, lightings, and viewing vectors. This rotaton/flip transformation can be represented by the following matrix F:

$$F = \begin{bmatrix} \mu & 0 & 0 \\ 0 & 1 & 0 \\ 0 & 0 & 1 \end{bmatrix} \begin{bmatrix} \cos\phi & -\sin\phi & 0 \\ \sin\phi & \cos\phi & 0 \\ 0 & 0 & 1 \end{bmatrix} = \begin{bmatrix} \mu\cos\phi & -\mu\sin\phi & 0 \\ \sin\phi & \cos\phi & 0 \\ 0 & 0 & 1 \end{bmatrix}, \tag{1}$$

where μ is binary number taking 1 or -1, accounting for a reflection, and ϕ is the rotaional angle around the z-axis. By transforming the solution of Eq. (4) ($[\boldsymbol{n}_0, \ldots, \boldsymbol{n}_{N-1}], [\boldsymbol{l}_0, \ldots, \boldsymbol{l}_{L-1}]$) by using this matrix F, we can obtain another candidate $F[\boldsymbol{n}_0, \ldots, \boldsymbol{n}_{N-1}], F[\boldsymbol{l}_0, \ldots, \boldsymbol{l}_{L-1}]$ without changing the reprojection error of Eq. (4), because it does not change the relationship of these vectors.

However, by enforcing an integrability constraint, the rotation/flip ambiguity is solved remaining a convex/concave ambiguity. This constraint can be enforced by minimizing the integrability cost below:

$$\min_F E_{itg} = \sum_i \left| \frac{\partial}{\partial y}\left(\frac{n^F_{i,x}}{n^F_{i,z}}\right) - \frac{\partial}{\partial x}\left(\frac{n^F_{i,y}}{n^F_{i,z}}\right) \right|^2, \tag{2}$$

where $[n^F_{i,x}, n^F_{i,y}, n^F_{i,z}]^{\mathrm{T}} \triangleq F\boldsymbol{n}_i$ and $\boldsymbol{n}_i$ is the solution of Eq. (4). The integrability cost can be minimized by a linear search.

However, the integrability costs corresponding to some ϕ is the same as that of $\phi + \pi$. Thus, this results in the convex/concave ambiguity as in [2]. It cannot be disamguated without information such as the cast shadow, boundary, and user selection.

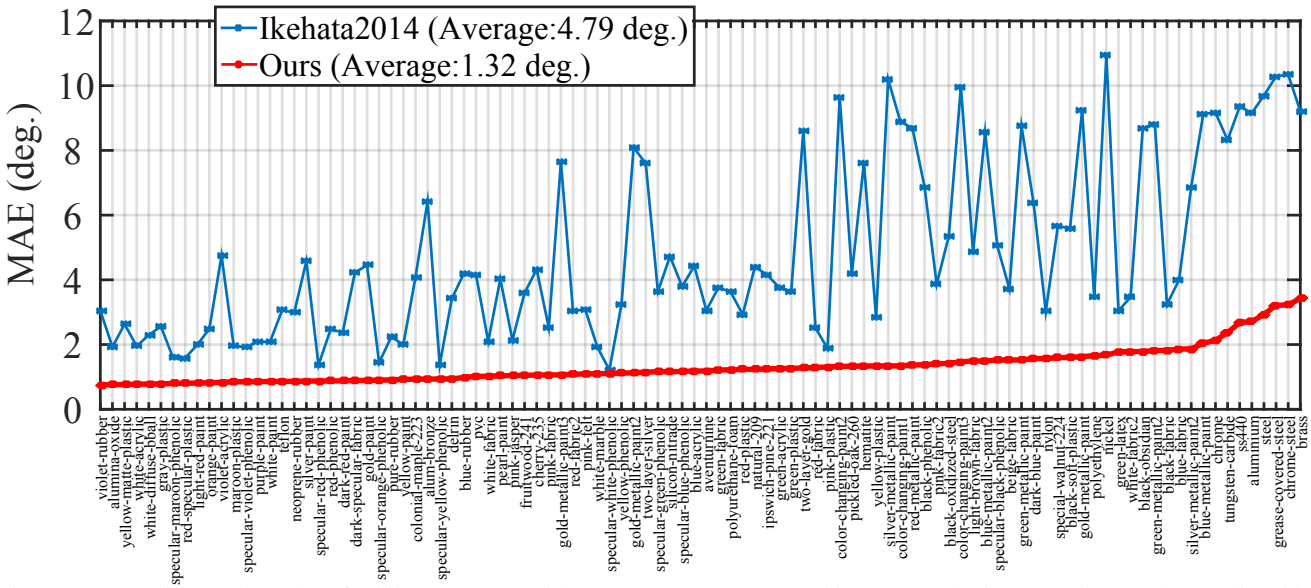

Figure 1: Experimental results of calibrated case, with 100 MERL BRDFs (45 images each, *bunny*). The results are listed in ascending order of Ours.

2. Evaluation for Calibrated Photometric Stereo with MERL BRDFs

We evaluated our calibrated photometric stereo for 100 different BRDFs in the MERL database, as described in Sec. 6.5. The parameter setting and evaluation method were the same as that in Sec. 6.5 but we used 45 test images here. As in Sec 6.4, we used 99 BRDFs for PCA for each test, omitting the BRDF for the test images.

The result is shown in Fig. 1. The average errors over the 100 BRDFs were 4.79° (Ikehata2014 [1]) and 1.32° (ours), respectively. Our method greatly outperformed the compared method for the all tests. We emphasize that our method works very well with such a small number of images.

3. Detail of Results of Experiments in Sec. 6.4

In this Section, we provide the detailed results of our experiment of Sec. 6.4 of our submission in the following Fig. 2 to Fig. 101 for the hundred different materials. In each figure, the top row shows the normal maps of ground-truth and those recovered by using the methods of Sato2007 [4], Lu2013 [2], Lu2015 [3], and ours. The bottom row shows the input image and their error maps.

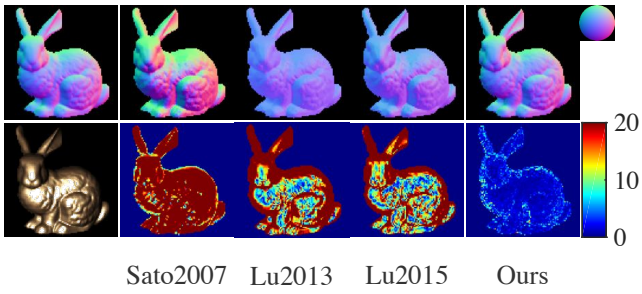

Figure 2: The results for alum-bronze.

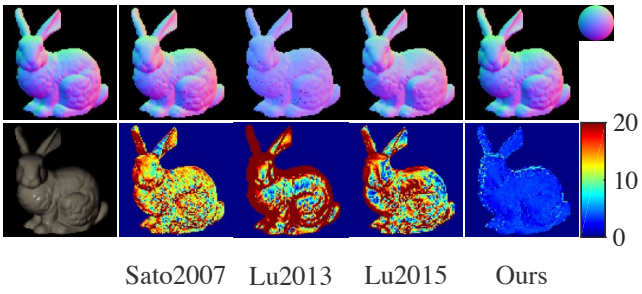

Figure 3: The results for alumina-oxide.

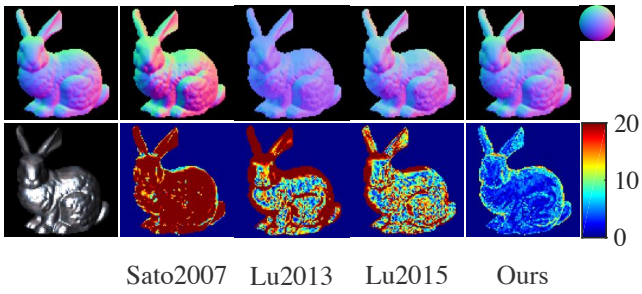

Figure 4: The results for aluminium.

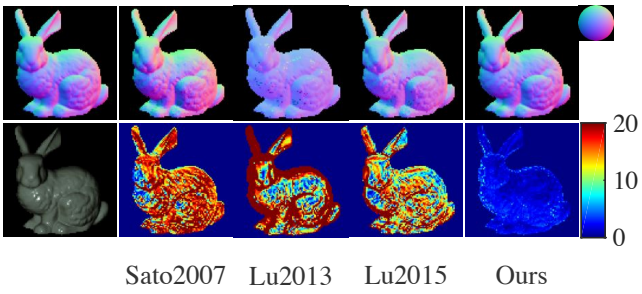

Figure 5: The results for aventurnine.

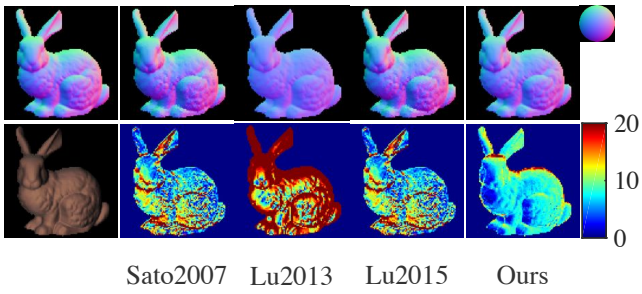

Figure 6: The results for beige-fabric.

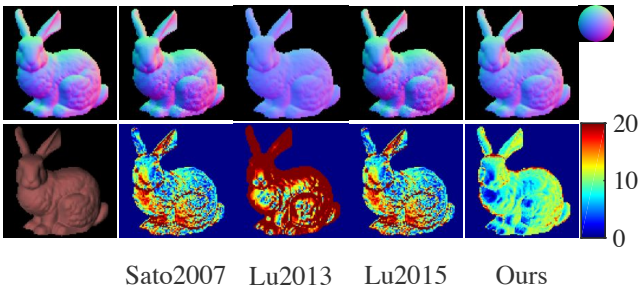

Figure 7: The results for black-fabric.

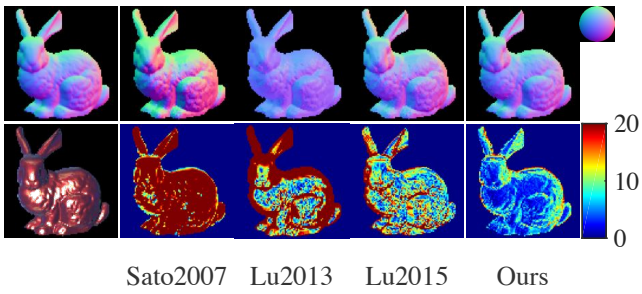

Figure 8: The results for black-obsidian.

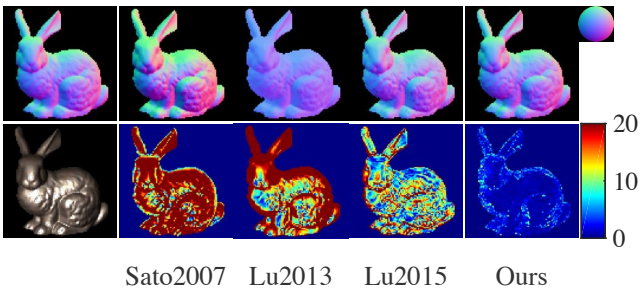

Figure 9: The results for black-oxidized-steel.

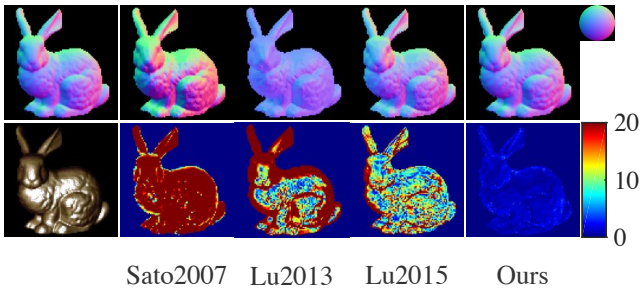

Figure 10: The results for black-phenolic.

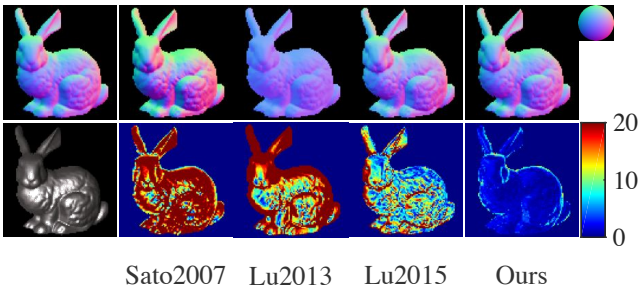

Figure 11: The results for black-soft-plastic.

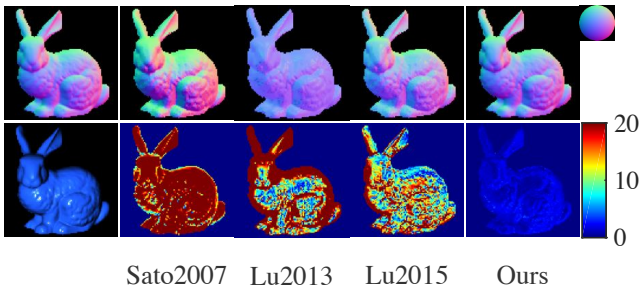

Figure 12: The results for blue-acrylic.

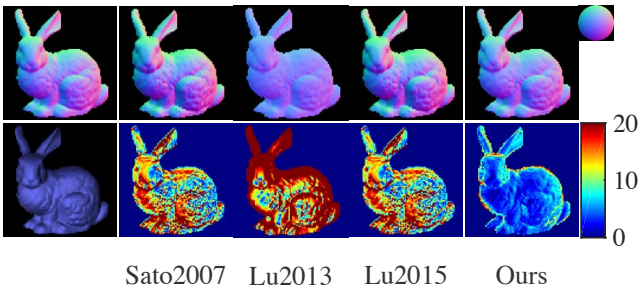

Figure 13: The results for blue-fabric.

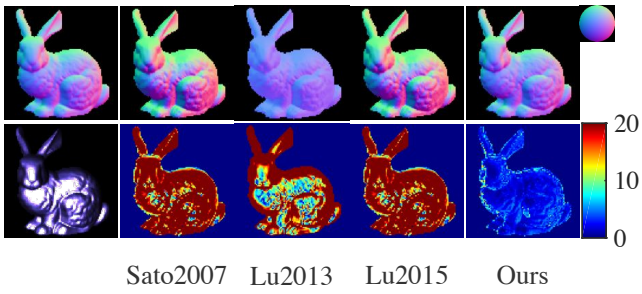

Figure 14: The results for blue-metallic-paint.

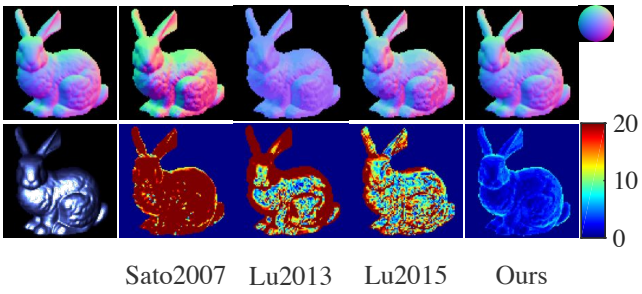

Figure 15: The results for blue-metallic-paint2.

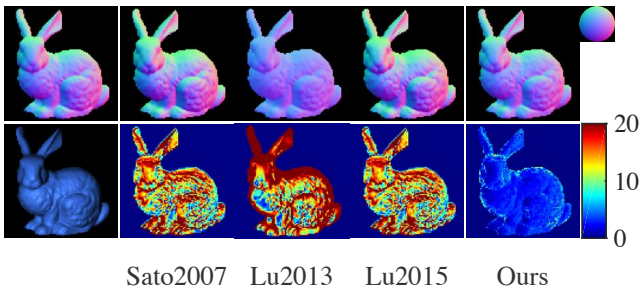

Figure 16: The results for blue-rubber.

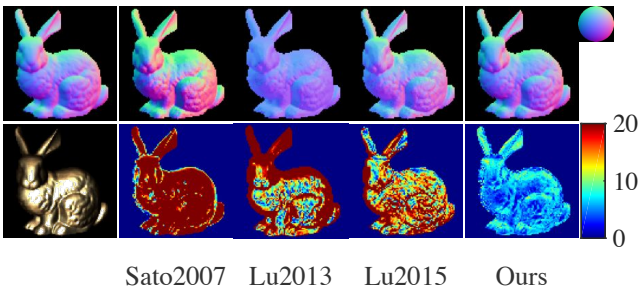

Figure 17: The results for brass.

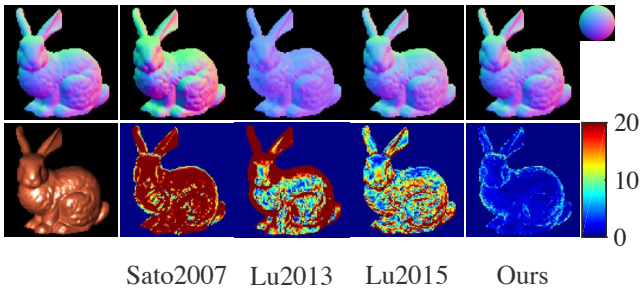

Figure 18: The results for cherry-235.

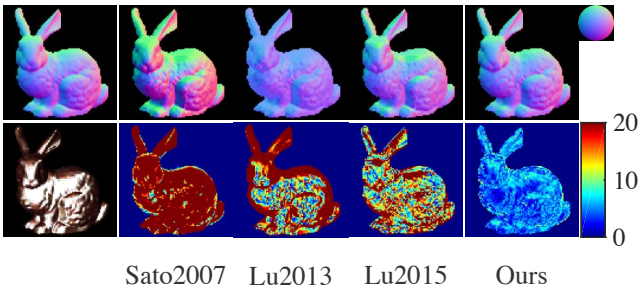

Figure 19: The results for chrome-steel.

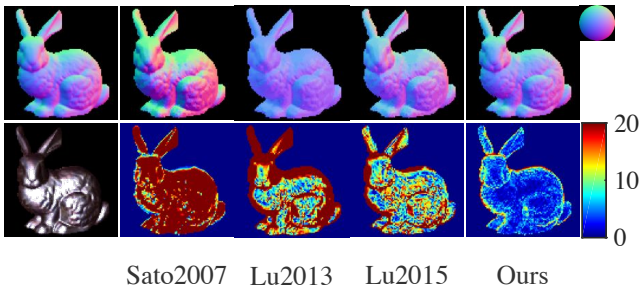

Figure 20: The results for chrome.

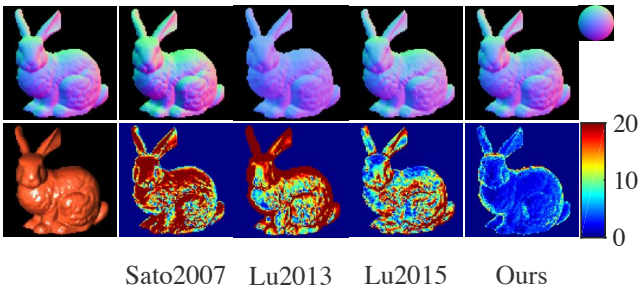

Figure 21: The results for colonial-maple-223.

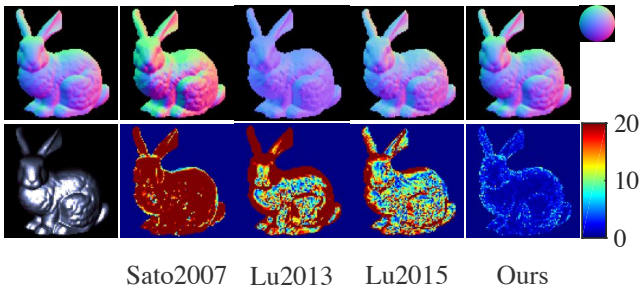

Figure 22: The results for color-changing-paint1.

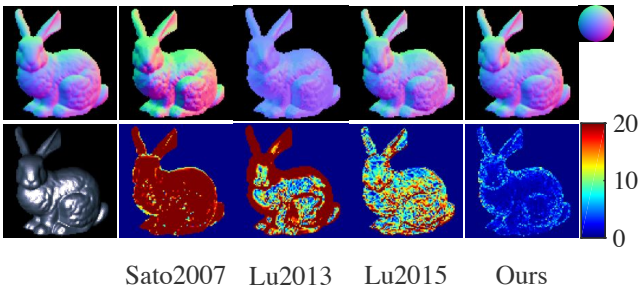

Figure 23: The results for color-changing-paint2.

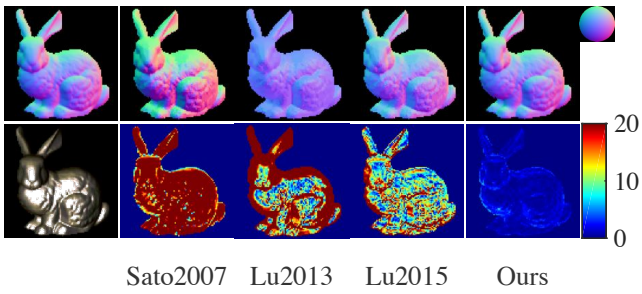

Figure 24: The results for color-changing-paint3.

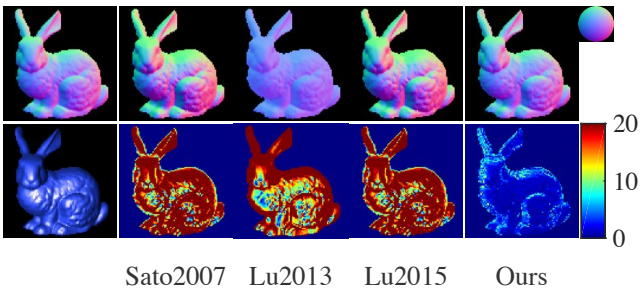

Figure 25: The results for dark-blue-paint.

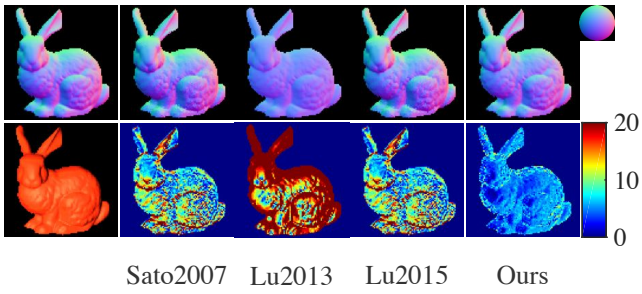

Figure 26: The results for dark-red-paint.

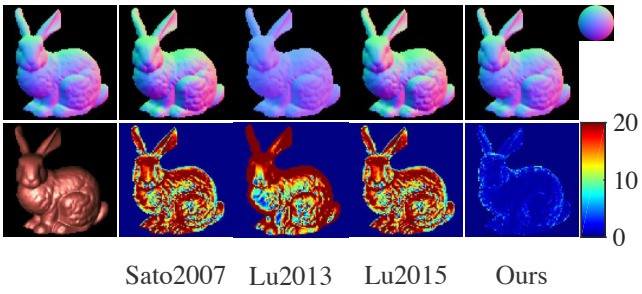

Figure 27: The results for dark-specular-fabric.

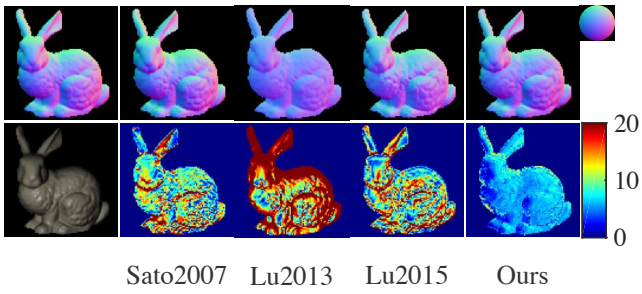

Figure 28: The results for delrin.

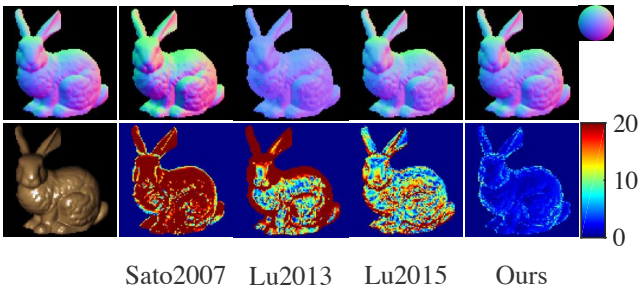

Figure 29: The results for fruitwood-241.

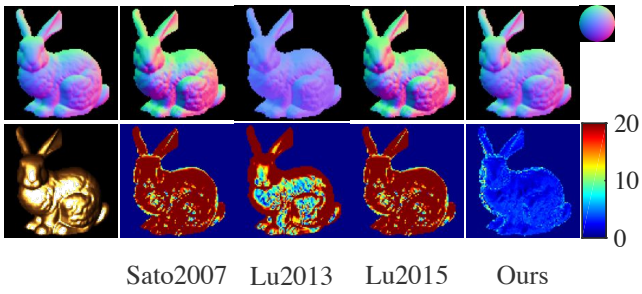

Figure 30: The results for gold-metallic-paint.

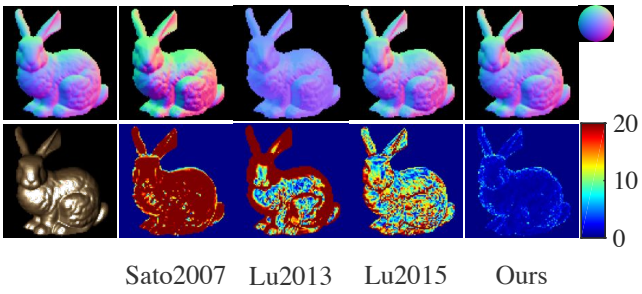

Figure 31: The results for gold-metallic-paint2.

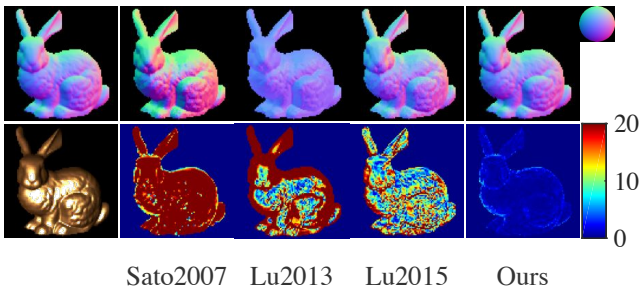

Figure 32: The results for gold-metallic-paint3.

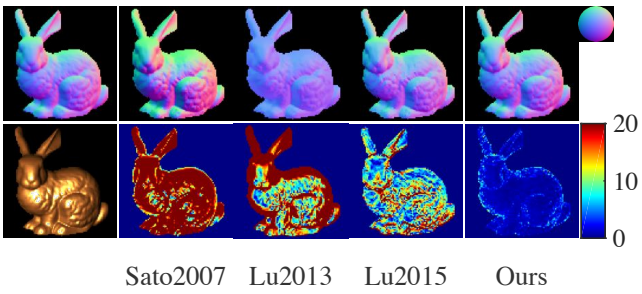

Figure 33: The results for gold-paint.

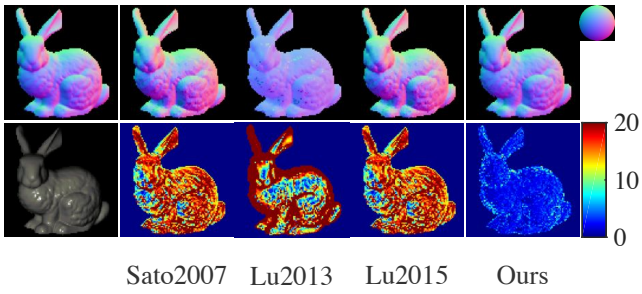

Figure 34: The results for gray-plastic.

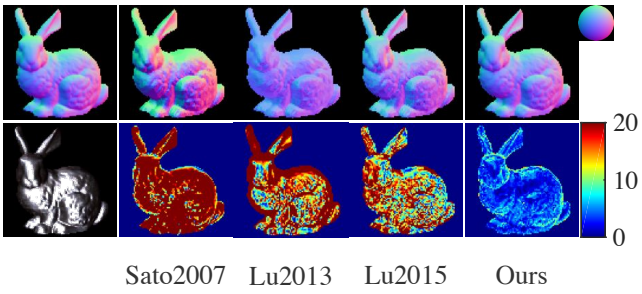

Figure 35: The results for grease-covered-steel.

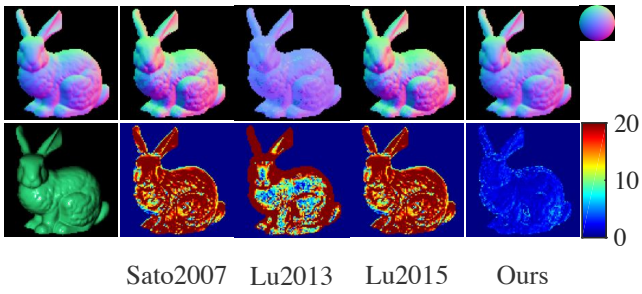

Figure 36: The results for green-acrylic.

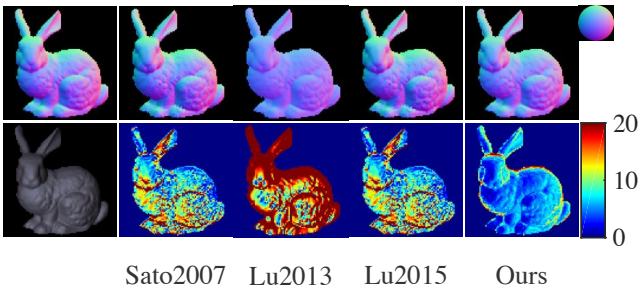

Figure 37: The results for green-fabric.

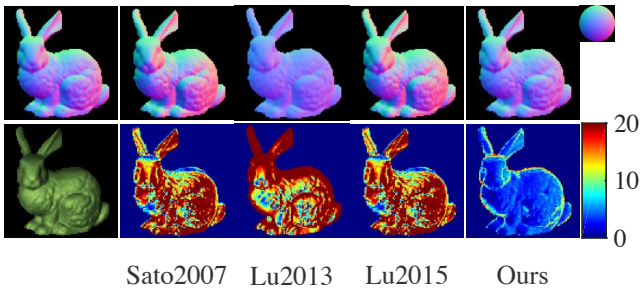

Figure 38: The results for green-latex.

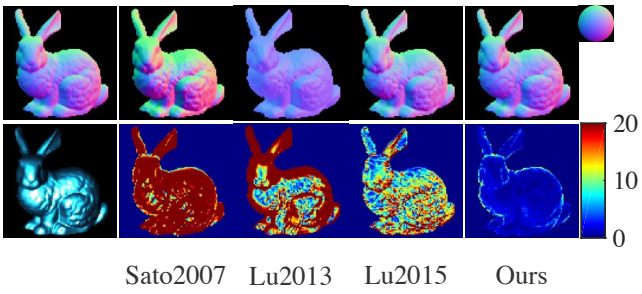

Figure 39: The results for green-metallic-paint.

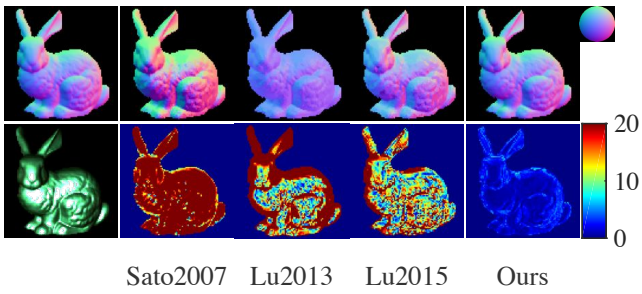

Figure 40: The results for green-metallic-paint2.

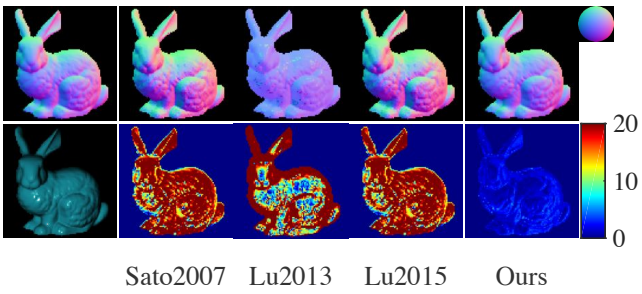

Figure 41: The results for green-plastic.

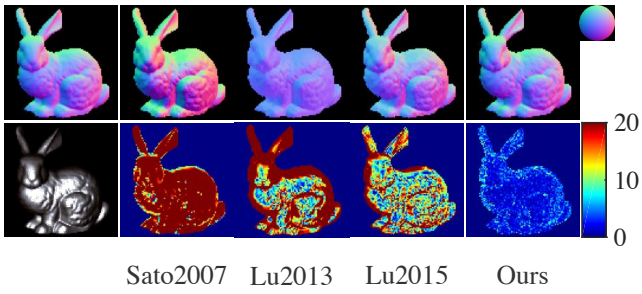

Figure 42: The results for hematite.

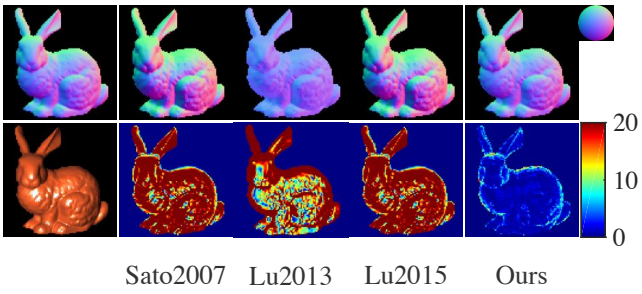

Figure 43: The results for ipswich-pine-221.

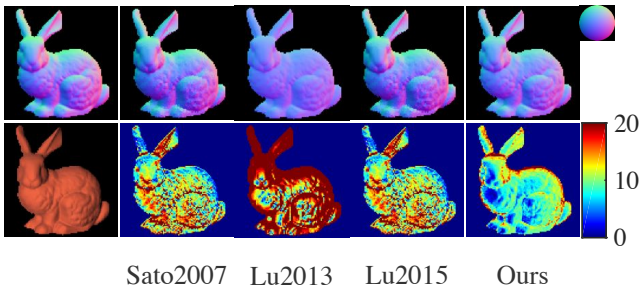

Figure 44: The results for light-brown-fabric.

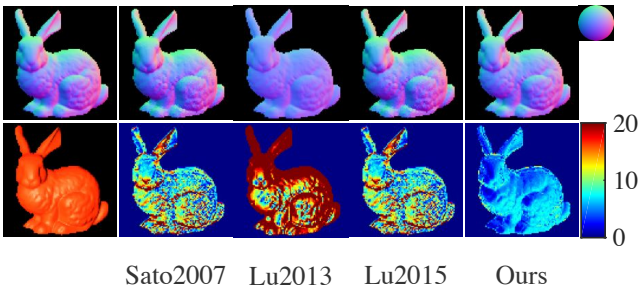

Figure 45: The results for light-red-paint.

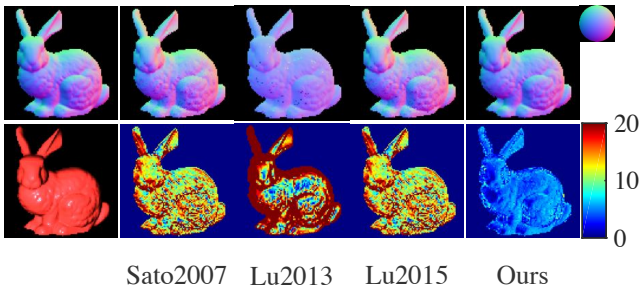

Figure 46: The results for maroon-plastic.

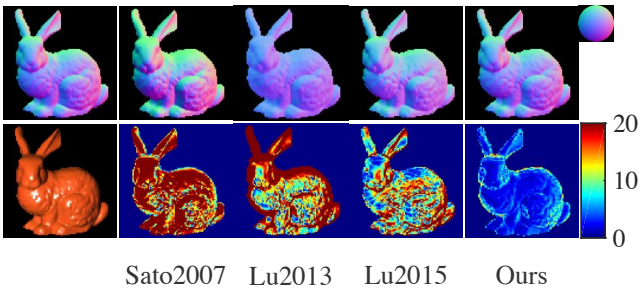

Figure 47: The results for natural-209.

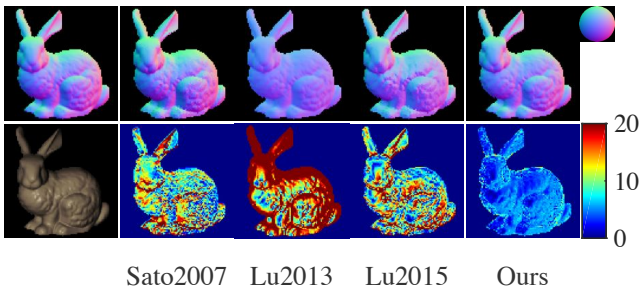

Figure 48: The results for neoprene-rubber.

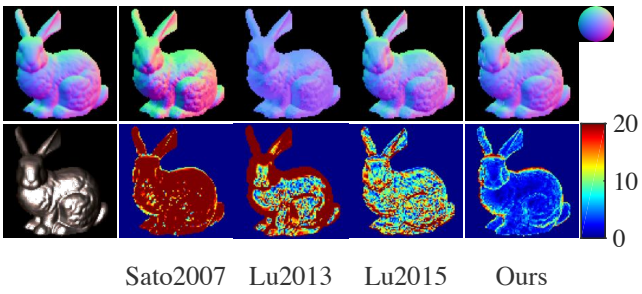

Figure 49: The results for nickel.

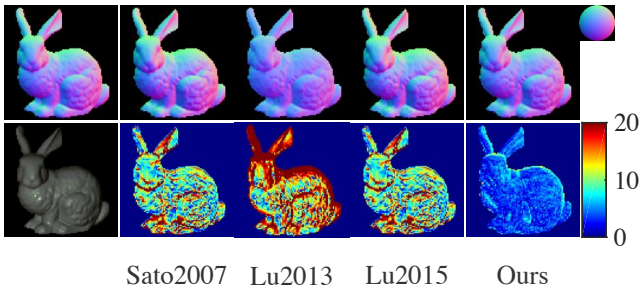

Figure 50: The results for nylon.

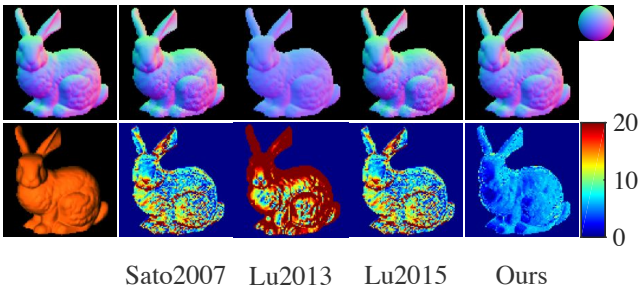

Figure 51: The results for orange-paint.

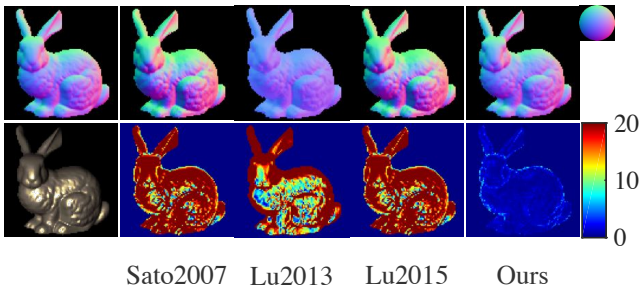

Figure 52: The results for pearl-paint.

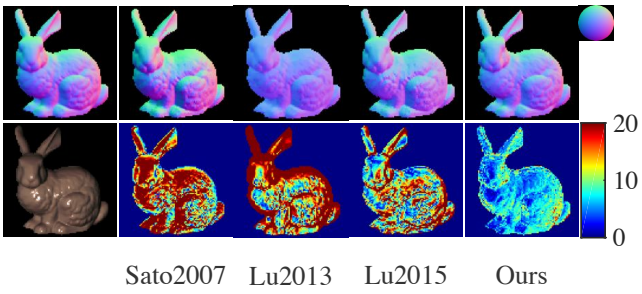

Figure 53: The results for pickled-oak-260.

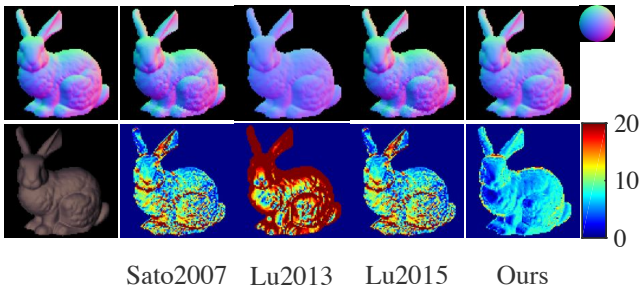

Figure 54: The results for pink-fabric.

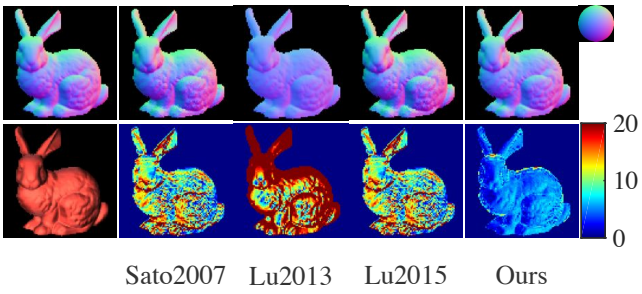

Figure 55: The results for pink-fabric2.

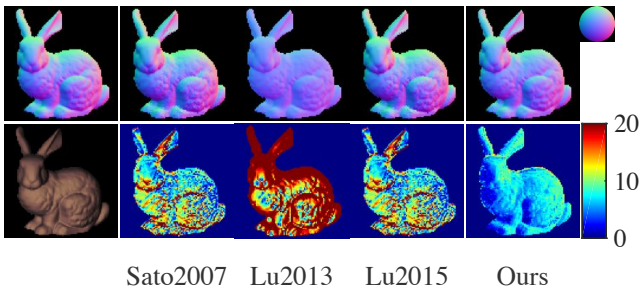

Figure 56: The results for pink-felt.

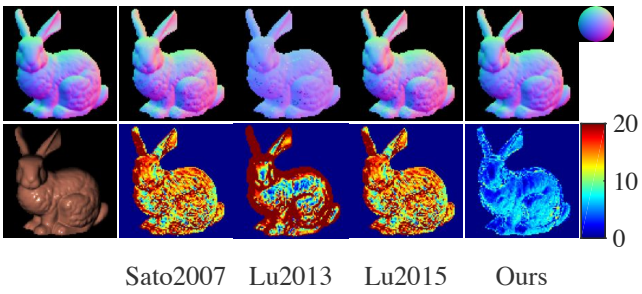

Figure 57: The results for pink-jasper.

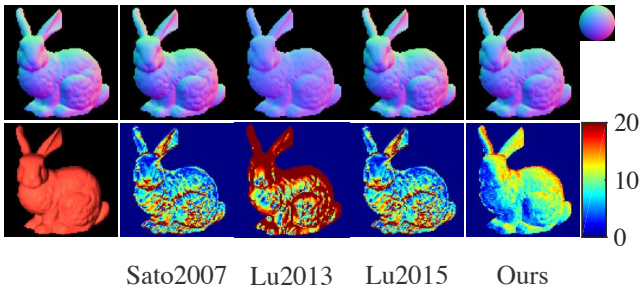

Figure 58: The results for pink-plastic.

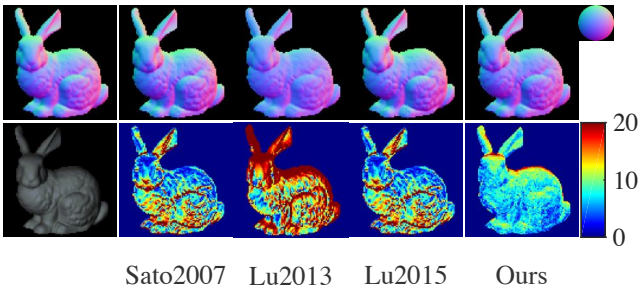

Figure 59: The results for polyethylene.

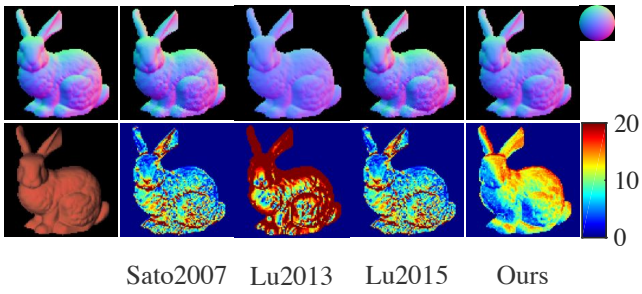

Figure 60: The results for polyurethane-foam.

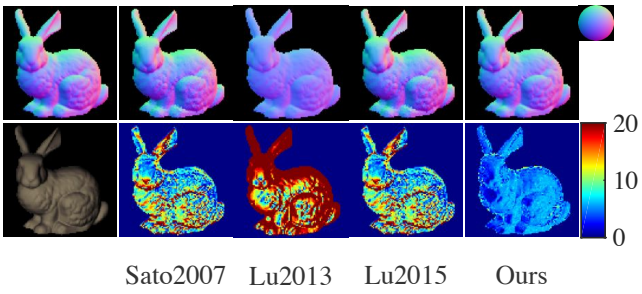

Figure 61: The results for pure-rubber.

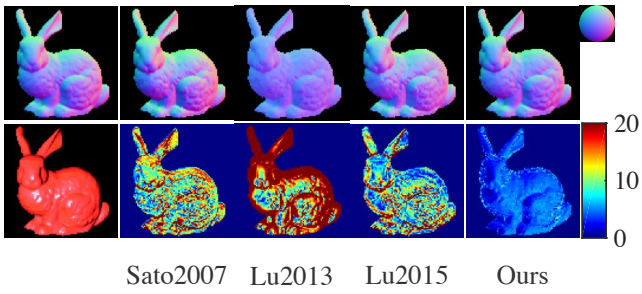

Figure 62: The results for purple-paint.

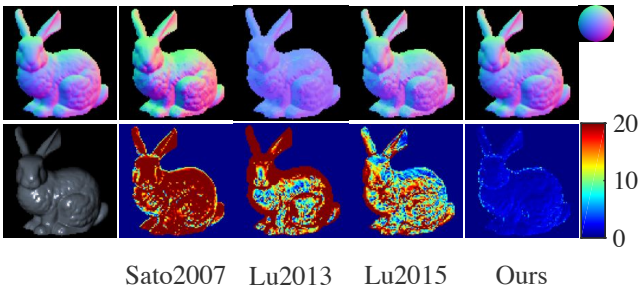

Figure 63: The results for pvc.

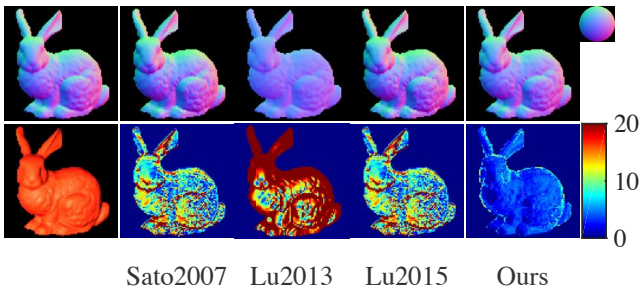

Figure 64: The results for red-fabric.

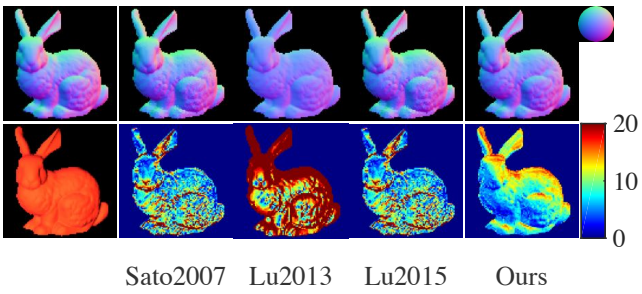

Figure 65: The results for red-fabric2.

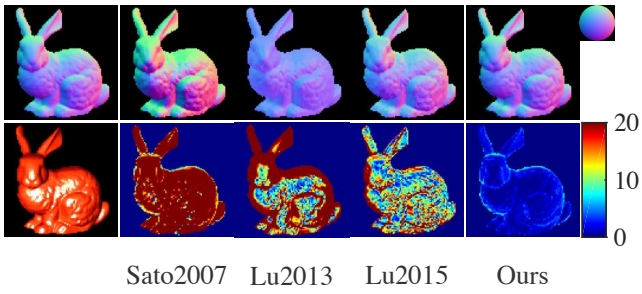

Figure 66: The results for red-metallic-paint.

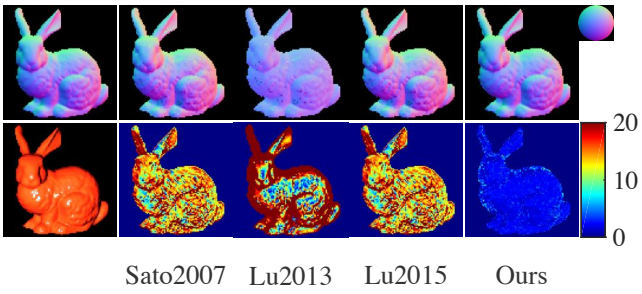

Figure 67: The results for red-phenolic.

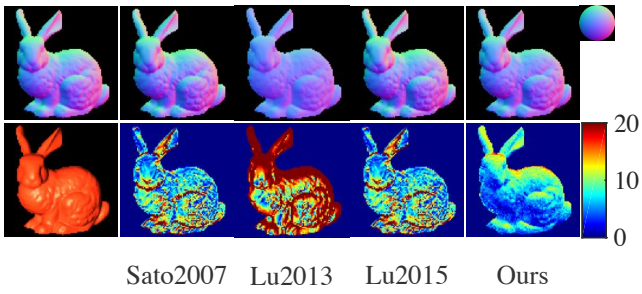

Figure 68: The results for red-plastic.

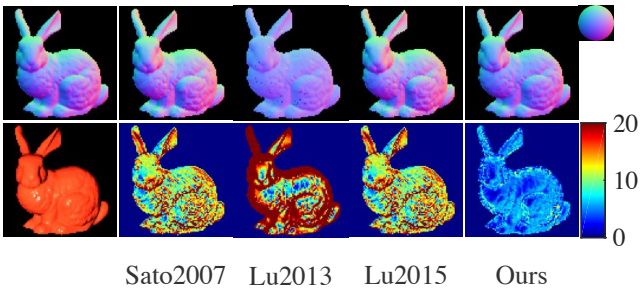

Figure 69: The results for red-specular-plastic.

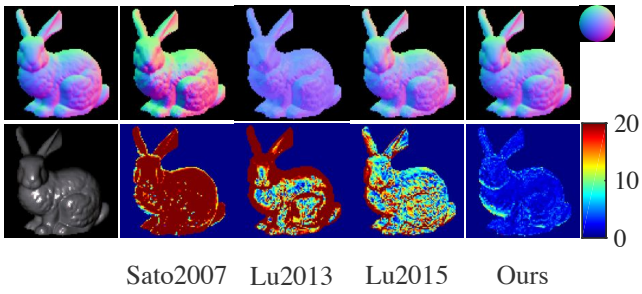

Figure 70: The results for silicon-nitrade.

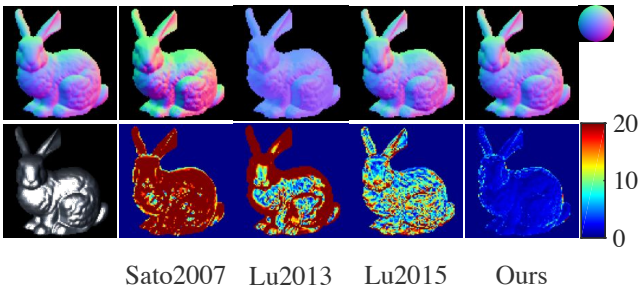

Figure 71: The results for silver-metallic-paint.

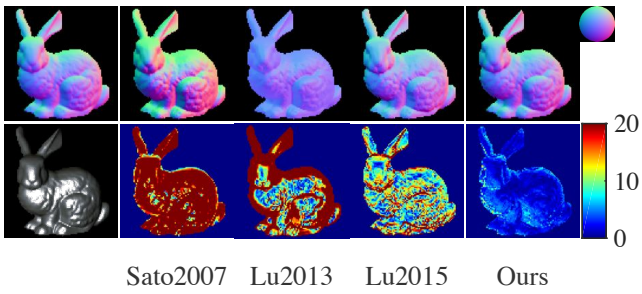

Figure 72: The results for silver-metallic-paint2.

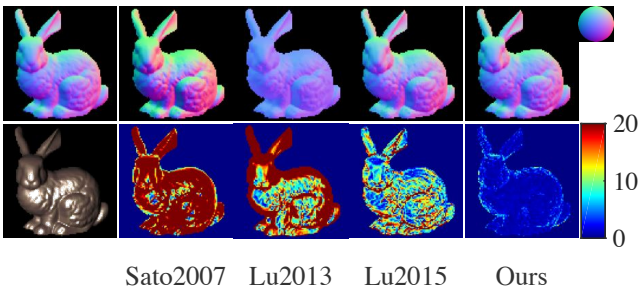

Figure 73: The results for silver-paint.

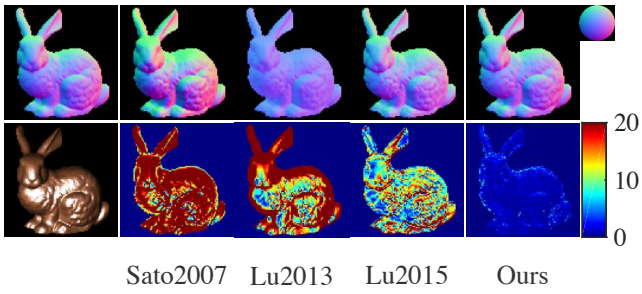

Figure 74: The results for special-walnut-224.

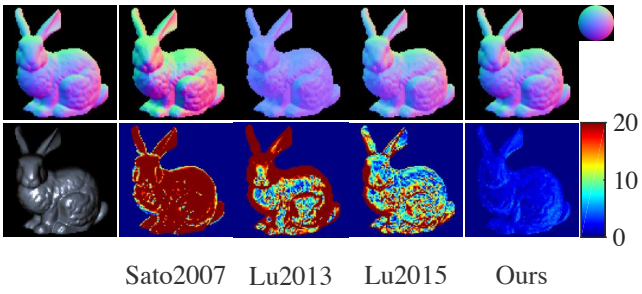

Figure 75: The results for specular-black-phenolic.

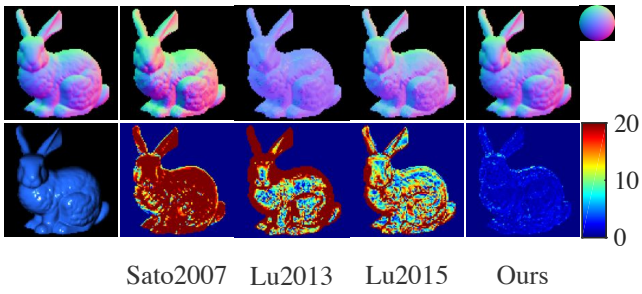

Figure 76: The results for specular-blue-phenolic.

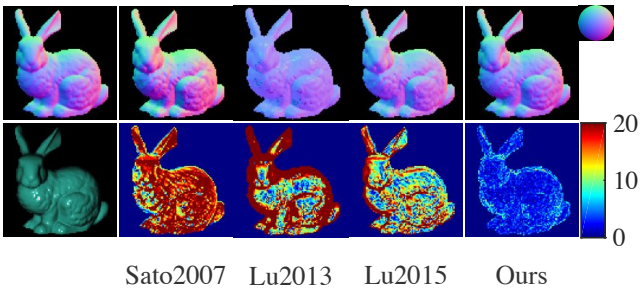

Figure 77: The results for specular-green-phenolic.

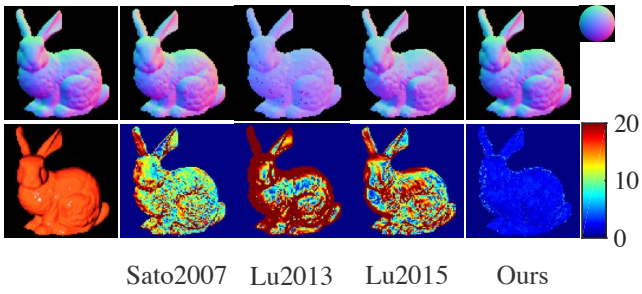

Figure 78: The results for specular-maroon-phenolic.

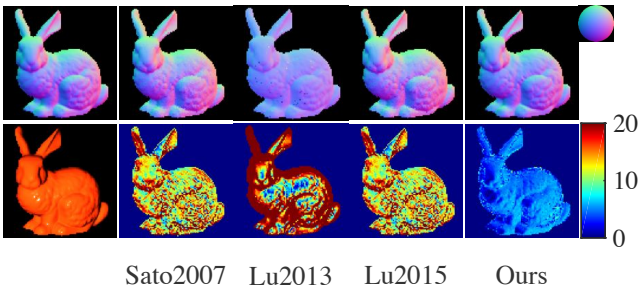

Figure 79: The results for specular-orange-phenolic.

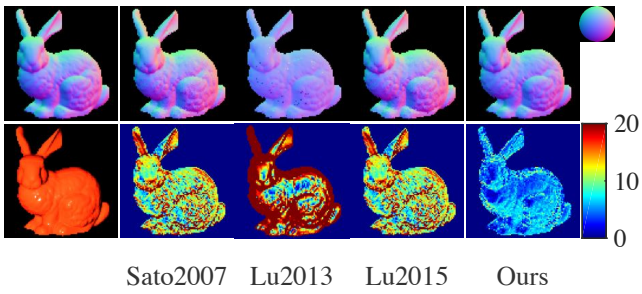

Figure 80: The results for specular-red-phenolic.

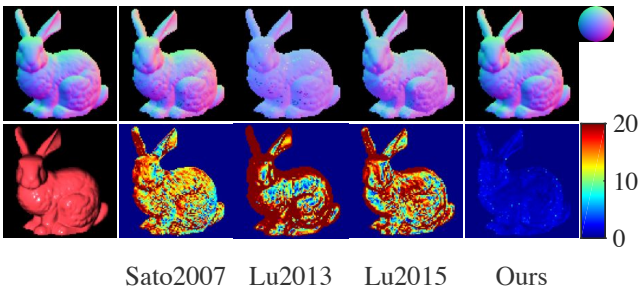

Figure 81: The results for specular-violet-phenolic.

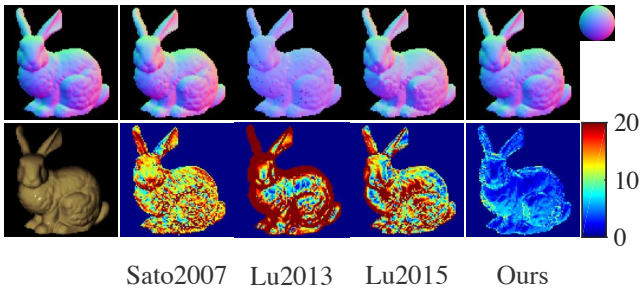

Figure 82: The results for specular-white-phenolic.

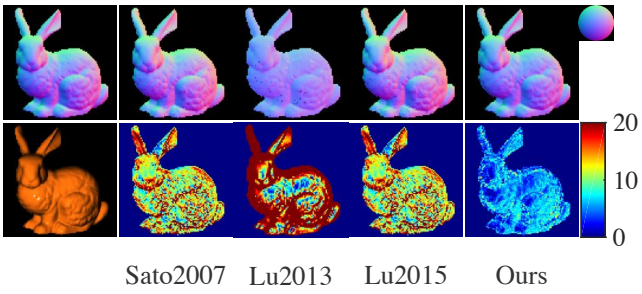

Figure 83: The results for specular-yellow-phenolic.

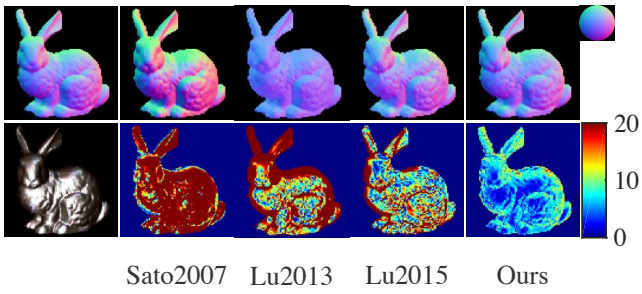

Figure 84: The results for ss440.

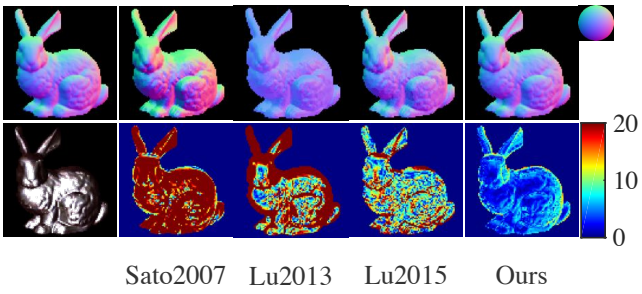

Figure 85: The results for steel.

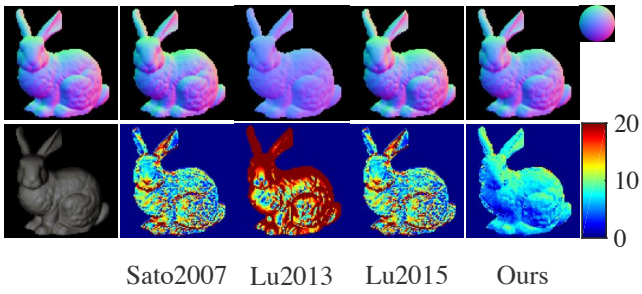

Figure 86: The results for teflon.

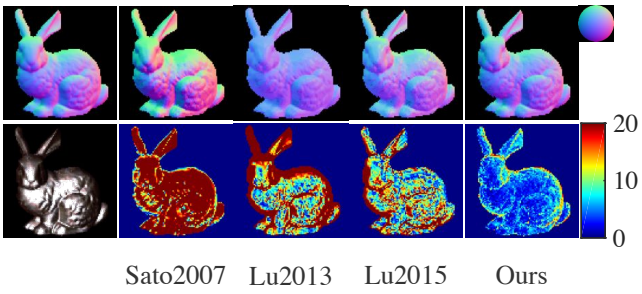

Figure 87: The results for tungsten-carbide.

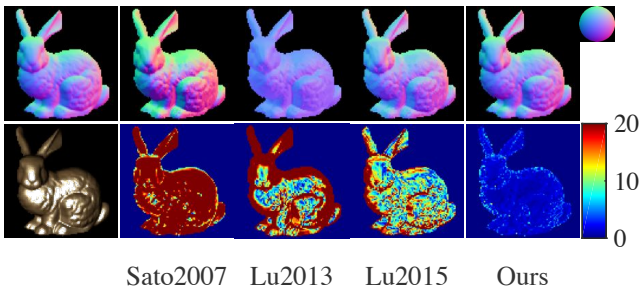

Figure 88: The results for two-layer-gold.

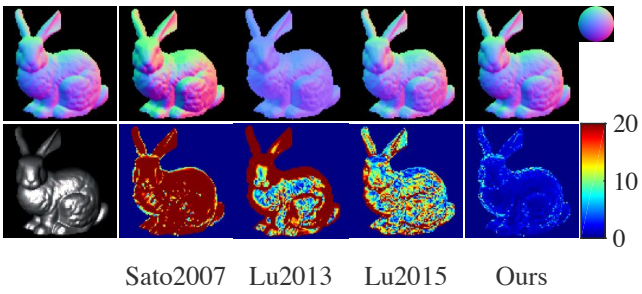

Figure 89: The results for two-layer-silver.

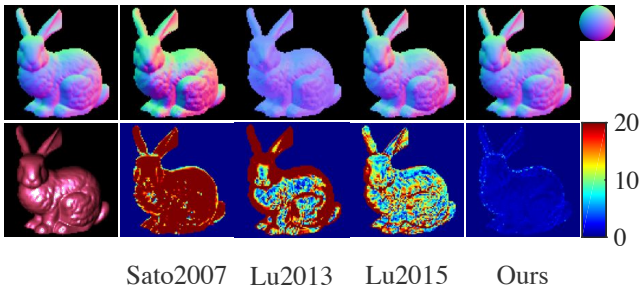

Figure 90: The results for violet-acrylic.

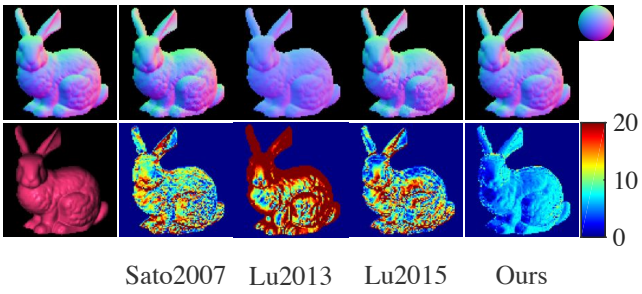

Figure 91: The results for violet-rubber.

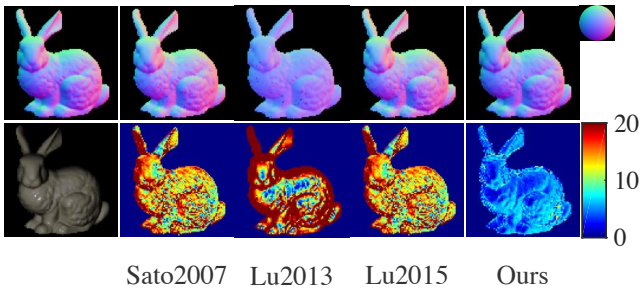

Figure 92: The results for white-acrylic.

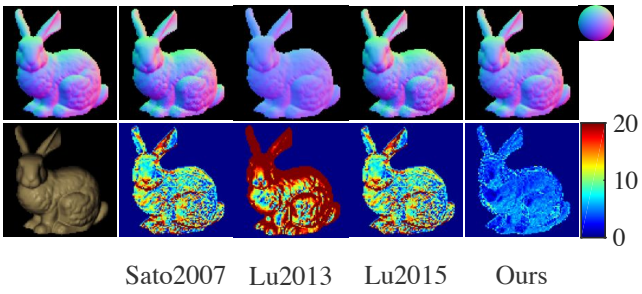

Figure 93: The results for white-diffuse-bball.

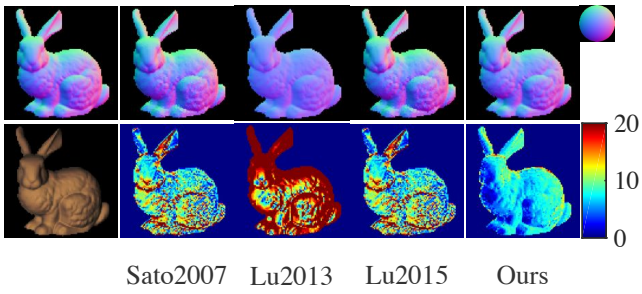

Figure 94: The results for white-fabric.

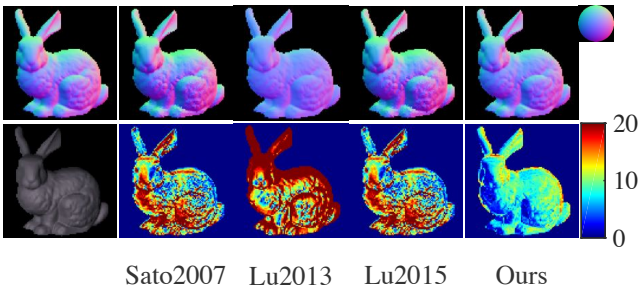

Figure 95: The results for white-fabric2.

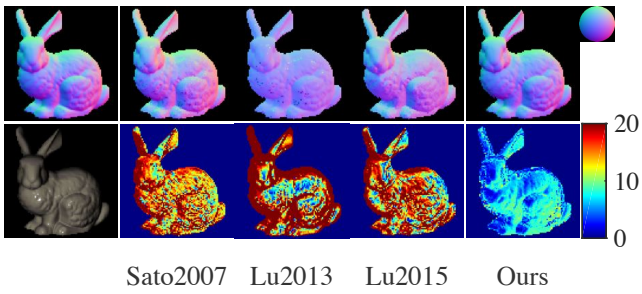

Figure 96: The results for white-marble.

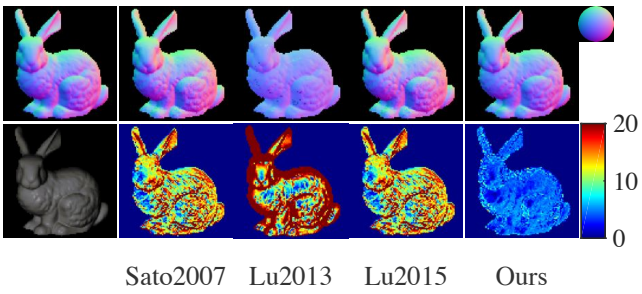

Figure 97: The results for white-paint.

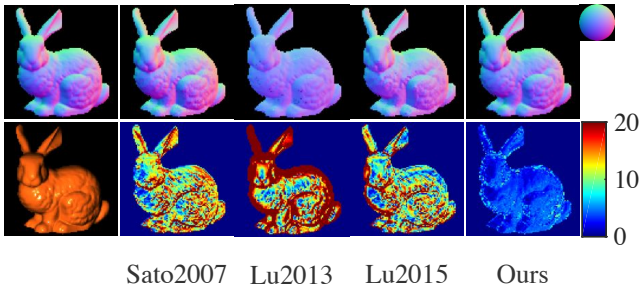

Figure 98: The results for yellow-matte-plastic.

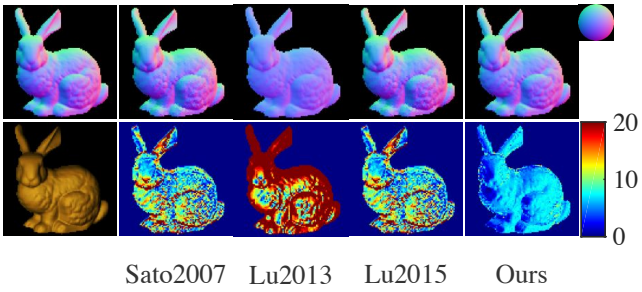

Figure 99: The results for yellow-paint.

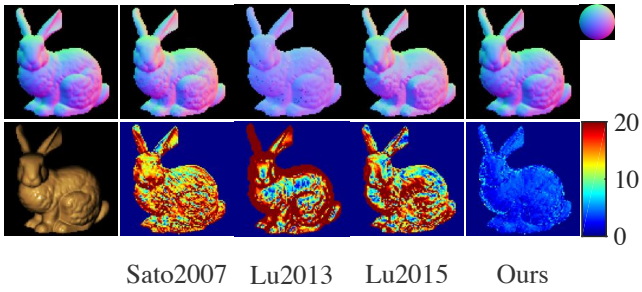

Figure 100: The results for yellow-phenolic.

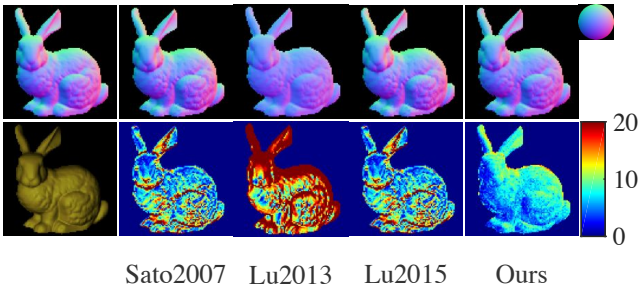

Figure 101: The results for yellow-plastic.

References

[1] S. Ikehata and K. Aizawa. Photometric stereo using constrained bivariate regression for general isotropic surfaces. In *Proc. CVPR*, 2014. 2

[2] F. Lu, Y. Matsushita, I. Sato, T. Okabe, and Y. Sato. Uncalibrated photometric stereo for unknown isotropic reflectances. In *Proc. CVPR*, 2013. 1, 2

[3] F. Lu, I. Sato, and Y. Sato. Uncalibrated photometric stereo based on elevation angle recovery from brdf symmetry of isotropic materials. In *Proc. CVPR*, 2015. 2

[4] I. Sato, T. Okabe, Q. Yu, and Y. Sato. Shape reconstruction based on similarity in radiance changes under varying illumination. In *Proc. ICCV*, 2007. 2